Silicon Radicals in Silicon Oxynitride: A Theoretical ESR Study

Lonnie D. Crosby and Henry A. Kurtz*

Computational Research On Materials Institute, CROMIUM, Department of Chemistry, The University of Memphis, Memphis, Tennessee 38152

Received: January 6, 2006; In Final Form: April 11, 2006

Quantum mechanical calculations are performed on a series of silicon radical defects. These are the ↑ Si ≡ $O_{3-x}N_x$, ↑ Si ≡ $N_{3-x}Si_x$, and ↑ Si ≡ $Si_{3-x}O_x$ defects, where x takes on values between 0 and 3. The defects under study constitute a central silicon radical, ↑ Si, with differing first-nearest-neighbor substitution, as may be found at a Si/SiO_xN_y interface. These first-nearest neighbor atoms are connected to the silicon radical via three single covalent bonds, denoted as "≡". A hybrid defect, ↑ Si≡ONSi, is also included. Calculations are performed on gas-phase-like cluster models, as well as more-constrained hybrid quantum and molecular mechanical (QM/MM) models. The isotropic hyperfine coupling constants of these defects are calculated via density functional theory (DFT). Trends in these calculated hyperfines are consistent between the different models utilized. Analysis of the electronic structure and geometries of defects correlate well with trends in the electronegativity of the first-nearest-neighbor atoms. Changes in radical hybridization, induced by changes in the first-nearest-neighbor composition, are the primary factor that affects the calculated hyperfines. Furthermore, comparisons to experimental results are encouraging. Agreement is found between experiments on amorphous to crystalline materials.

1. Introduction

Microelectronics are an integral part of life today. The most prolific of these devices is the metal-oxide semiconductor field-effect transistor (MOSFET). Its uses include volatile memory and integrated circuits. The MOSFET makes use of standard silicon/silicon dioxide technology, and device reliability is related to the properties of these materials. An important example is that potential charge carriers, either native or induced, degrade performance.[1] A set of defects related to this effect have been identified as P_b centers[2,3] and are located at the Si/SiO_2 interface. These interface traps[4] can act as electron traps at this interface. Another subset of charge carriers can act as border traps[4] at some distance from this interface. These may include the hemi-E′[5] center and various partially oxidized silicon radicals, $\cdot SiO_{3-x}Si_x$. The boron dopant used in the silicon substrate and polysilicon gate can also be a potential charge carrier.[1] Boron migration into the Si/SiO_2 interface can lead to trap formation. Currently, low-concentration nitrogen dopants are used to reduce the extent of boron diffusion. This nitration changes the nature of the Si/SiO_2 interface. The effective interface is Si/SiO_xN_y where the subscripts x and y are used to illustrate the nonstoichiometric nature of the silicon oxynitride material. With such an interface, new silicon radical defects are possible. Similar to the partially oxidized radicals, these defects constitute partially nitrated silicon radicals, $\cdot SiO_{3-x}N_x$ and $\cdot SiSi_{3-x}N_x$.

The detection of paramagnetic defects, such as these silicon radical point defects, is generally accomplished via electron spin resonance (ESR) spectroscopy. The most significant feature of the ESR spectra of these silicon radicals is the ^{29}Si hyperfine coupling constant. This interaction can be as large as 500 G. Experimental studies have been performed on α-quartz,[6] silica glass,[7] α-Si:H,[8] α-SiO_2,[9,10] and Si/SiO_2[11] systems. Silicon nitride has also been studied with ESR spectroscopy.[12,13] However, few studies have been performed on SiO_xN_y or Si/SiO_xN_ysystems.

Theoretical studies of ESR hyperfine splittings have proven to be important in identifying the nature of defects. The hemi-E′ and P_b centers have been studied computationally.[14] Karna et al. have studied the partially oxidized silicon radicals, $\cdot SiO_{3-x}Si_x$.[14] However, the partially nitrated silicon radicals have not been studied, except the K center by Pacchioni.[15] These calculations are typically done utilizing cluster models or models with periodic boundary conditions. The methods used include unrestricted Hartree−Fock (UHF) theory and density functional theory (DFT). Recent papers have illustrated the effectiveness of DFT calculations on the calculation of hyperfine splittings.[16,17]

The goal of this paper is to determine the isotropic hyperfine coupling constants of various silicon radical defects with differing first-nearest-neighbor composition. These hyperfines will be compared to the experiment, when applicable, and provide guidance to future experimental research.

1.1. Silicon Defects. The defects studied all consist of a central silicon radical with varying first-nearest-neighbor composition, which will be a combination of O, N, and Si atoms. The full set can be viewed as a triad, where the vertexes are formed by monosubstituted radicals. The oxygen, nitrogen, and silicon variants are well-documented as the hemi-E′-, K-, and P_b-centers, respectively.[2,3,5,12,13] Each leg of the triad connects two of these vertexes, such that traveling along its length sequentially substitutes the first-nearest-neighbor atoms. This triad is shown in Figure 1 with legs labeled according to substitution. Starting from the top and proceeding clockwise, the hemi-E′-center is a fully oxidized silicon radical, $\cdot SiO_3$. The first leg introduces oxygen−nitrogen substitutions to form the K-center. The K-center consists of a completely nitrated silicon radical, $\cdot SiN_3$. The second leg introduces nitrogen−silicon substitutions to form the P_b center. This center is composed of

* Author to whom correspondence should be addressed. E-mail: hkurtz@memphis.edu.

10.1021/jp060117v CCC: $33.50
Published on Web 06/17/2006

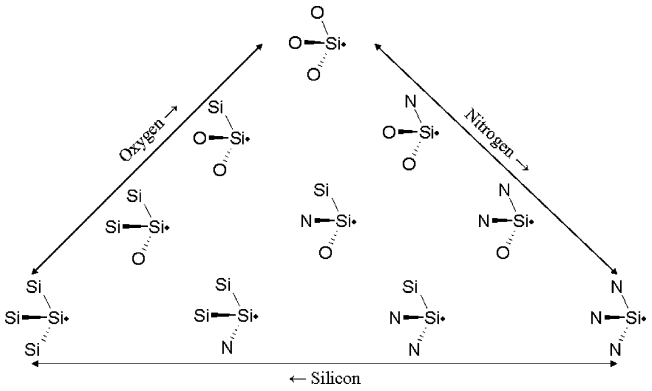

Figure 1. Diagrammatic representation of the possible silicon radicals in silicon oxynitride with different first-nearest-neighbor substitution. Only the silicon radical and its first-nearest neighbors are shown.

a silicon radical surrounded by Si atoms, $\cdot SiSi_3$. The last leg introduces silicon−oxygen substitution to reform the hemi-E′-center. The central defect in this figure is a hybrid structure that is composed of all three atoms associated with a silicon radical, ·SiONSi.

2. Methodology

In this work, cluster models terminated with H atoms were used to represent the silicon defects. These models include first-, second-, and third-nearest-neighbor atoms from the silicon radical. Because of the inherently nondendritic nature of silicon, silicon dioxide, silicon nitride, and silicon oxynitride materials, the nearest-neighbor scheme becomes cumbersome in some cases. As a result, additional atoms were added to complete ring or plane features. Two differing optimization methods were applied to construct the models that have been used.

The first is a completely gas-phase-like cluster approximation, with each model independently built and optimized. The smallest clusters were built first, optimized, and then used to build the next-larger cluster with subsequent optimization. This method makes comparisons across the differing model sizes of a single defect difficult, because of a combination of geometric and electronic effects.

The second procedure eliminates geometrical changes between the differing sized clusters by the use of a hybrid quantum mechanical/molecular mechanical (QM/MM) method. This method uses a cluster larger than the third-nearest neighbor to perform the geometry optimization. This cluster is divided into two regions where QM and MM calculations are performed. The QM region contains the silicon radical and up to the third-nearest-neighbor atoms. During and after optimization, this QM region is saturated with hydrogen to eliminate the free valences associated with the partition. The resulting third-nearest-neighbor cluster is used to construct the smaller first- and second-nearest-neighbor clusters without further optimization. The second-nearest-neighbor cluster is constructed by removing the hydrogen terminators and replacing the third-nearest-neighbor atoms with hydrogen. The bond lengths associated with the newly added H atoms are adjusted to acceptable values. The values used were 1.510, 0.980, and 1.030 Å for the Si−H, O−H, and N−H bonds, respectively. The first-nearest-neighbor cluster is constructed via a similar procedure were the hydrogen terminators and third-nearest-neighbor atoms are removed. The second-nearest-neighbor atoms are replaced with hydrogen and bond lengths are adjusted as described previously. The added H atoms are positioned to align along the bonds of the initial third-nearest-neighbor cluster. This method produces clusters that have the same local geometry around the silicon radical as the initial third-nearest-neighbor cluster.

The adjusted bond lengths used for this method could also be independently optimized from the rest of the cluster. A calculation of the first-nearest-neighbor ·SiONSi cluster has been performed with independently optimized hydrogen bond lengths. The resulting bond lengths were shorter by an average of 0.022 Å. This gives bond lengths of 1.493, 0.954, and 1.007 Å for Si−H, O−H, and N−H bonds, respectively. However, this additional refinement did not change the results of the subsequent property analysis and, therefore, was not calculated for other clusters.

The environment in which these silicon radical defects are modeled is of some concern. The gas-phase-like clusters are significantly more flexible than the more-constrained QM/MM clusters. This constraint can be mild with an amorphous environment or strict with a crystalline environment. The environment used for the amorphous case is a silicon dioxide-like stoichiometry for atoms past the first-nearest neighbor. This choice produces the mildest constraints on the system and removes environmental effects from an inconsistent description of this surrounding environment.

Clusters were optimized at the DFT level of theory using the B3LYP[18] hybrid correlation and exchange functional. The standard SBKJC[19] effective core potentials and basis sets were used with an additional *d* polarization function[20] for all atoms except hydrogen. The GAMESS defaults were used with exponents of 0.395 on Si and 0.8 on O and N atoms. The QM/MM[21] calculation utilized the same theory and basis for the QM partition. The MM partition was optimized using the MM3 force field. The GAMESS[22] quantum chemistry program was utilized to perform the QM calculations. An optional GAMESS add-in, Tinker,[21] was used to perform the MM calculations.

A property calculation was performed on each of the clusters produced. The property of interest is the spin density, $\delta_{\alpha-\beta}$, at the nuclear positions, r_i, in the cluster (eq 1). This requires calculation of the α and β electron densities at nuclear positions.

$$\delta_{\alpha-\beta}(r_i) = \sum_{\mu\in\alpha}\langle\mu|\delta(r-r_i)|\mu\rangle - \sum_{\nu\in\beta}\langle\nu|\delta(r-r_i)|\nu\rangle \qquad (1)$$

These densities will be positive or negative, depending on excess α or β character. The spin densities at these positions were used to calculate the isotropic hyperfine coupling constant associated with each magnetic nucleus through the use of the Fermi-contact operator, which describes the interaction energy of electrons in contact with a nucleus.

$$A_0 = \frac{8\pi}{3} g_e\beta_e g_n\beta_n \delta_{\alpha-\beta}(r_i) \qquad (2)$$

The constant terms g_e, g_n, β_e, and β_n refer to the electronic *g*-factor, nuclear *g*-factor, bohr magneton, and nuclear magneton, respectively. The isotropic hyperfine coupling constant, A_0, is shown in eq 2. This expression is independent of the spin multiplicity of the nucleus. However, the nuclear spin must be nonzero for the hyperfine spectra to be observable. The electronic multiplicity of the radical does have an effect on the hyperfine spectra. A multiplicative term, $^1/_2\ \sum S^{-1}$, is needed in eq 2 to account for this effect. The previous expression assumes a doublet electronic state, which is sufficient for the radicals in this study. The isotropic hyperfine coupling constant may also have a positive or negative sign. This sign is determined in eq 2 by the signs of the spin density and the nuclear *g*-factor. The sign of this hyperfine coupling constant is difficult to measure

TABLE 1: Reported Isotropic Hyperfine Coupling Constants (A_0) of Silicon Radicals, Using Gas-Phase-Like Clusters[a]

Legend																			
Cluster		·SiO_3			·SiO_2N			·SiONSi				·$SiON_2$			·$SiSi_3$		·$SiNSi_2$			·SiN_2Si			·SiN_3	
Isotope		$^{29}Si\uparrow$	^{17}O		$^{29}Si\uparrow$	^{17}O	^{14}N	$^{29}Si\uparrow$	^{17}O	^{14}N	^{29}Si	$^{29}Si\uparrow$	^{17}O	^{14}N	$^{29}Si\uparrow$	^{29}Si	$^{29}Si\uparrow$	^{14}N	^{29}Si	$^{29}Si\uparrow$	^{14}N	^{29}Si	$^{29}Si\uparrow$	^{14}N
1 NN A_0		-361	-37, -14, -14		-311	-45, -8	4	-212	-26	1	-66	-263	-16	3, 12	-93	2, 2, 2	-134	2	-22, -21	-171	0, 6	-70	-213	4, 4, 5
2 NN A_0		-402	-28, -26, -26		-382	-40, -20	13	-197	-19	5	-104	-304	-13	10, 16	-106	-1, -1, 0	-125	2	-22, -22	-178	3, 7	-62	-298	10, 10, 10
3 NN A_0		-423	-32, -26, -20		-380	-25, -18	13	-192	-17	4	-89	-371	-19	10, 13	-46	9, 11, 11	-137	2	-26, -25	-200	4, 6	-75	-379	9, 9, 9

[a] These gas-phase-like clusters include first-, second-, and third-nearest-neighbor substitution. The hyperfines are reported in units of gauss and were calculated via DFT/B3LYP and the TZV+d basis. The upward arrow symbol (↑) denotes the silicon radical center.

experimentally and relates to the ordering of nuclear spin states. Calculated hyperfines are given with sign; however, they are discussed and compared to experiment via their absolute values.

The nuclei of interest are ^{29}Si, ^{14}N, and ^{17}O, which constitute the silicon radical and its first-nearest neighbors. ^{17}O is included in the results, although its low abundance would make experimental observation difficult. The spin density was calculated at each magnetic nucleus at the DFT level of theory, using the B3LYP[18] hybrid correlation and exchange functional. The basis set used was the all-electron TZV[23] basis with an additional *d* polarization function[20] for all atoms except hydrogen, TVZ+d. The GAMESS defaults were once again used with exponents of 0.388 on Si, 0.98 on N, and 1.28 on O atoms. GAMESS[22] was again used to perform these calculations.

3. Results

3.1. Gas-Phase-Like Scheme. The method referenced here as the gas-phase-like method uses a layer approach to build and optimize the defect clusters. This method produces small, flexible clusters that differ in local geometry around the silicon radical. Table 1 reports the isotropic hyperfine coupling constants of selected magnetic nuclei in these gas-phase-like models. Hyperfines are reported for the silicon radical nucleus as well as the first-nearest-neighbor ^{29}Si, ^{17}O, and ^{14}N nuclei. The ·SiO_2Si and ·$SiOSi_2$ defects are not given here, because they have been previously calculated from gas-phase-like clusters.[14]

The effects of cluster size can readily be observed for each defect by comparing the hyperfine values for the first-, second-, and third-nearest-neighbor models. The absolute value of these hyperfines may increase or decrease as the sizes of the particular clusters change. The absolute change in these values upon moving from the first- to second-nearest-neighbor clusters is generally larger than the change upon moving between the second- and third-nearest-neighbor clusters. This convergence is encouraging and demonstrates the localized nature of the radical.

Considering the absolute changes of the hyperfine on the silicon radical nuclei of these defects, half have a change of 7−15 G and 5−6 G between the first- and second-nearest-neighbor and between the second- and third-nearest-neighbor clusters, respectively. The defects from the ·SiO_3 to ·SiN_3 centers show much-greater changes of 41−85 G between the first- and second-nearest-neighbor models. This is due to the flexibility of the O and N first-nearest-neighbor atoms within these clusters. This does not affect clusters with more rigid Si atoms in the first-nearest-neighbor shell. Also, much larger changes are observed between the second- and third-nearest-neighbor models of 21−81 G. These are observed for the ·SiO_3, ·$SiON_2$, ·SiN_3, and ·SiN_2Si defects. This change is mild for the ·SiO_3 and ·SiN_2Si defects (21−22 G) and more severe for the remaining two defects. At the third-nearest-neighbor level, the extremities of these model clusters are beginning to become crowded, as a result of the dendritic method used to build these models. This lack of secondary structure is a severe shortcoming most evident by the low hyperfine value of the third-nearest neighbor ·$SiSi_3$ defect (−46 G). Crowding has made the silicon radical in this cluster significantly more planar than in the first- or second-nearest-neighbor models.

Using the third-nearest-neighbor results, several trends are apparent, in comparison of the absolute value of the isotropic hyperfines between different defects. Starting with the silicon radical nuclei, the hyperfine decreases from the ·SiO_3 to ·SiN_3 defects, as oxygen is replaced by nitrogen. The hyperfine also decreases upon replacement of nitrogen by silicon, going from the ·SiN_3 to ·$SiSi_3$ defects. The hyperfine, conversely, increases from the ·$SiSi_3$ to ·SiO_3 defects, as silicon is replaced by oxygen, utilizing the previously reported values from ref 14. The magnitudes of the changes across each section are 44, 333, and 377 G, respectively. The lower first step is attributed to the similarity between the electronegativity of oxygen and nitrogen and the dramatic difference in the other two steps is caused by the large difference in electronegativity between the N and Si or Si and O atoms.

The ·SiONSi defect has a hyperfine between that of the ·SiN_3 and ·SiN_2Si defects. The ·SiONSi and ·SiN_3 defects differ by an O → N and Si → N substitution. The O → N substitution is expected to affect the hyperfine less than the Si → N substitu-

TABLE 2: Reported Isotropic Hyperfine Coupling Constants (A_0) of Silicon Radicals, Using the QM/MM Scheme[a]

Legend	·SiO_3		·SiO_2Si			·SiO_2N			·$SiOSi_2$			·$SiONSi$			·$SiON_2$			·$SiSi_3$		·$SiNSi_2$			·SiN_2Si			·SiN_3	
Cluster Isotope	$^{29}Si\uparrow$	^{17}O	$^{29}Si\uparrow$	^{17}O	^{29}Si	$^{29}Si\uparrow$	^{17}O	^{14}N	$^{29}Si\uparrow$	^{17}O	^{29}Si	$^{29}Si\uparrow$	^{17}O	^{14}N	$^{29}Si\uparrow$	^{17}O	^{14}N	$^{29}Si\uparrow$	^{29}Si	$^{29}Si\uparrow$	^{14}N	^{29}Si	$^{29}Si\uparrow$	^{14}N	^{29}Si	$^{29}Si\uparrow$	^{14}N
1 NN A_0	-537	-58, -55, -46	-232	-13, -8	-83	-322	-15, -15	19	-135	-3	-18, -16	-218	-14	8	-67	-284	-3	15, 20	-75	4, 4, 5	-118	2	-8, -2	-169	2, 9	-38	-261	8, 14, 14
2 NN A_0	-459	-42, -42, -34	-221	-11, -7	-128	-327	-15, -14	13	-138	-4	-36, -22	-193	-10	6	-111	-305	-7	10, 15	-78	-1, 2, 8	-119	3	-20, -14	-173	3, 6	-68	-289	7, 10, 11
3 NN A_0	-452	-41, -37, -33	-222	-9, -7	-115	-358	-15, -14	13	-132	-3	-27, -22	-192	-12	6	-92	-346	-7	11, 14	-72	1, 5, 7	-107	3	-16, -15	-174	3, 5	-58	-313	6, 9, 11

[a] These clusters were built and optimized using the QM/MM scheme and include first-, second-, and third-nearest-neighbor substitution. Hyperfines are reported in units of gauss and were calculated via DFT/B3LYP and the TZV+d basis. The upward arrow symbol (↑) denotes the silicon radical center.

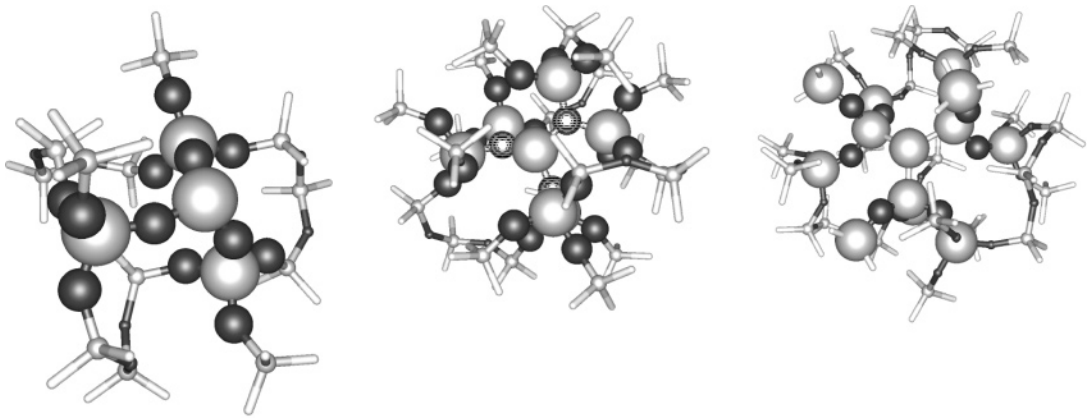

Figure 2. Quantum mechanical/molecular mechanical (QM/MM) models of the ·SiO_3, ·SiN_3, and ·$SiSi_3$ centers, displayed from left to right. The QM region of each model is the third-nearest neighbor and is illustrated by the portion rendered using a space fill model. The surrounding MM regions are displayed as ball-and-stick models. The silicon radical is located in the center of each picture. Light atoms are silicon, striped atoms are nitrogen, and dark atoms are oxygen. The environment is an amorphous silicon dioxide network.

tion. This latter substitution, according to the previously stated trends, increases the hyperfine. Table 1 shows that the ·SiONSi defect has a lower hyperfine than the ·SiN_3 defect, which agrees with these trends.

The first-nearest-neighbor nuclei generally have smaller-magnitude hyperfines and also follow the same trends as shown for the silicon radical nuclei. The first-nearest-neighbor nuclei also have varied hyperfines that are dependent on local structure and symmetry. The first-nearest-neighbor ^{17}O nuclei are generally not equivalent, with a spread of 6−7 G. The ^{29}Si and ^{14}N nuclei have a 1 G and 2−3 G spread, respectively. Also, these nuclei are equivalent or almost equivalent in ·$SiSi_3$ and ·SiN_3 defects. The difference between these spreads is attributed to the flexibility of oxygen as opposed to Si and N atoms.

The shortcomings of this model method are evident from the convergence problems of half of the defects studied. This results from an ever-changing local structure and lack of secondary structure. Expansion of these types of clusters beyond the third-nearest neighbor would only magnify these problems in structure.

3.2. QM/MM Scheme. The QM/MM method produces clusters that have been constrained by their environment. This is an attempt to better model the environment in a condensed-phase silicon dioxide-like network for all defects. This approach should eliminate some of the problems related to steric crowding of the gas-phase-like models at the third-nearest neighbor. Past this shell, some secondary structure is incorporated, including five- to six-membered Si−O rings. This method, as implemented, produces clusters that have similar local geometry around the silicon radical for the appropriate first-, second-, and third-nearest-neighbor clusters. Table 2 reports the isotropic hyperfines of selected magnetic nuclei for these QM/MM models. Hyperfines are shown for the silicon radical nucleus, as well as for the first-nearest-neighbor nuclei. Figure 2 shows the ·SiO_3, ·SiN_3, and ·$SiSi_3$ defects as they are used in this method. These models vary in size from 61 to 130 total atoms. Only 16−28 atoms are present in the QM portion.

The effect of cluster size on the calculated hyperfines can be observed by comparing the change of the hyperfine values between the first-, second-, and third-nearest-neighbor clusters.

This change, which is similar to that observed in the gas-phase-like model, does not have a definite direction. The hyperfine may increase or decrease as the models are enlarged. Also, the absolute change from the first- to second-nearest-neighbor clusters is mildly larger than the change from the second- to third-nearest-neighbor clusters. Once again, some models demonstrate larger-magnitude changes. Considering the silicon radical nuclei and determining the absolute changes in hyperfine due to changes in cluster size of these defects, most demonstrate a 1−11 G change from the first- to second-nearest-neighbor clusters and a 1−12 G change from the second- to third-nearest-neighbor clusters. These changes are essentially equal and are a result of the nonvarying nature of the local geometry. However, defects from the $\cdot SiO_3$ to $\cdot SiN_3$ centers show the much-larger changes of 21−78 G and 24−31 G from the first- to second-nearest neighbor and second- to third-nearest-neighbor clusters. Compared to the gas-phase models, these changes are lower in magnitude.

Several trends are apparent in comparing the hyperfine values across defects considering the third nearest neighbor clusters. Starting with the central silicon radical nucleus, the magnitude of the hyperfine decreases from the $\cdot SiO_3$ to $\cdot SiN_3$ defects. The magnitude also decreases from the $\cdot SiN_3$ to $\cdot SiSi_3$ defects, and it increases from the $\cdot SiSi_3$ to $\cdot SiO_3$ defects. The magnitudes of these changes are 139, 241, and 380 G, respectively. These trends are similar to those observed for the gas-phase-like models. The difference in magnitude is once again attributed to the differences in electronegativity between Si, O, and N atoms. The first-nearest-neighbor atoms have hyperfines that are in agreement with these trends.

The $\cdot SiONSi$ defect has a calculated hyperfine on the silicon radical between that of the $\cdot SiO_2Si$ and $\cdot SiOSi_2$ defects. The $\cdot SiONSi$ and $\cdot SiOSi_2$ defects differ by an N → Si substitution. According to the discussed trends, this substitution decreases the hyperfine. The $\cdot SiONSi$ defect has a higher hyperfine than $\cdot SiOSi_2$, which is consistent with the observed trends.

In this QM/MM method, first-nearest-neighbor nuclei are generally not equivalent. This is mostly due to the nature of the geometry constraint and the asymmetry that most of these defects possess. The spread of the hyperfines on these nuclei are comparable and, in the case of oxygen, smaller than that of the gas-phase-like method. Spreads for the first-nearest-neighbor silicon, oxygen, and nitrogen nuclei are 1−5 G, 1−4 G, and 2−3 G, respectively.

3.3. QM/MM Crystalline Environment. The $\cdot SiSi_3$, $\cdot SiN_3$, and $\cdot SiO_3$ defects are included in another QM/MM scheme, where they are built and optimized in their respective crystalline environments, rather than simulating silicon oxynitride. These environments are modeled as α-Si, α-Si_3N_4, and cristobalite, respectively. These models produce a cluster whose local geometry is conserved through the various cluster sizes and is the most structurally constrained model presented. Table 3 reports the isotropic hyperfine coupling constants of selected nuclei in these models. The silicon radical nucleus and the first-nearest-neighbor nuclei are included. Figure 3 also shows the $\cdot SiO_3$, $\cdot SiN_3$, and $\cdot SiSi_3$ defects as they are used in this method. These models are larger than the previous QM/MM models, which contain 123−183 total atoms. The QM portion remains similar in size, containing 16−28 atoms.

The effect of varying cluster size can one again be determined by the observation of the changes in calculated hyperfines between different-sized clusters. Similar to previous results, the direction of the change in these hyperfines between differently sized clusters are ambiguous. The changes between the first- and second-nearest-neighbor clusters are also generally larger than the changes between the second- and third-nearest-neighbor clusters. However, unlike previous methods, these changes are of similar magnitude across these three defects. Considering the absolute changes on the silicon radical nucleus, there is a 6−29 G and 10−15 G change between the first- and second-nearest-neighbor clusters and between the second- and third-nearest-neighbor clusters, respectively. This increased convergence is mostly due to the added constraint of being modeled in a crystalline environment.

TABLE 3: Reported Isotropic Hyperfine Coupling Constants (A_0) of Silicon Radicals in Crystalline Environments[a]

	−$SiSi_3$ Cluster		−SiN_3 Cluster		−SiO_3 Cluster	
isotope	$^{29}Si\uparrow$	^{29}Si	$^{29}Si\uparrow$	^{14}N	$^{29}Si\uparrow$	^{17}O
1NN A_0	−116	−1, −1, −1	−249	8, 11, 16	−445	−53, −32, −23
2NN A_0	−122	−3, −3, −3	−269	6, 8, 12	−416	−39, −27, −21
3NN A_0	−112	−3, −4, −3	−254	6, 7, 10	−428	−37, −29, −19

[a] These clusters were built and optimized using the QM/MM scheme and include first-, second-, and third-nearest-neighbor substitution. Hyperfines are reported in units of gauss and were calculated via DFT/B3LYP and the TZV+d basis. The upward arrow symbol (↑) denotes the silicon radical center.

Trends are also observable in Table 3 by comparing the calculated hyperfines across these three defects. The observed trends in the silicon radical nucleus' hyperfine as a function of first-nearest-neighbor composition is the same as that reported in the gas-phase-like and QM/MM methods. The magnitudes of these changes are 174, 142, and 316 G, respectively, for the $\cdot SiO_3$ to $\cdot SiN_3$, $\cdot SiN_3$ to $\cdot SiSi_3$, and $\cdot SiSi_3$ to $\cdot SiO_3$ defects. This is reminiscent of the previous results, except for the 142 G change between the $\cdot SiN_3$ to $\cdot SiSi_3$ defects. This anomaly is caused by the low magnitude of the hyperfine on the $\cdot SiN_3$ defect, as compared to the other methods. First-nearest-neighbor nuclei are also not generally equivalent for N and O atoms. The silicon nuclei are equivalent in the $\cdot SiSi_3$ defect, because of the symmetry of that crystalline structure. The spreads for the nitrogen and oxygen nuclei are 1−3 G and 8−10 G, respectively. This result is similar to the gas-phase-like results where the flexibility or asymmetry of the O atoms is observed.

3.4. Dependence Studies. The calculated isotropic hyperfine coupling constants for all defects have the potential to be dependent on the utilized level of theory and basis set. These dependencies have been explored using the QM/MM optimized $\cdot SiO_3$, $\cdot SiN_3$, and $\cdot SiSi_3$ centers from Table 2. The basis set dependence study uses the DFT/B3LYP level of theory and four different basis sets. The first is the basis set used in the previous calculations, the TZV+d basis. The second is an altered form of the TZV+d basis, differing only by the decontraction of the two largest exponent primitives in the first *s* function to produce a second function. This decontraction produces a more flexible description of the region near the nucleus. The third basis is the cc-pVTZ[24] basis, which incorporates functions of higher angular momentum than does the TZV+d basis. This basis should produce a more-accurate valence description of the system. However, the parts of the basis that describe the nuclear regions are highly contracted and are not very flexible. Therefore, an altered cc-pVTZ basis is used as the fourth basis set in this study. The altered cc-pVTZ basis set differs from the original only by the complete decontraction of the first *s* function to form several functions containing only a single primitive. Tests of different levels of theory utilize the TZV+d basis set and three different levels of theory. The methods

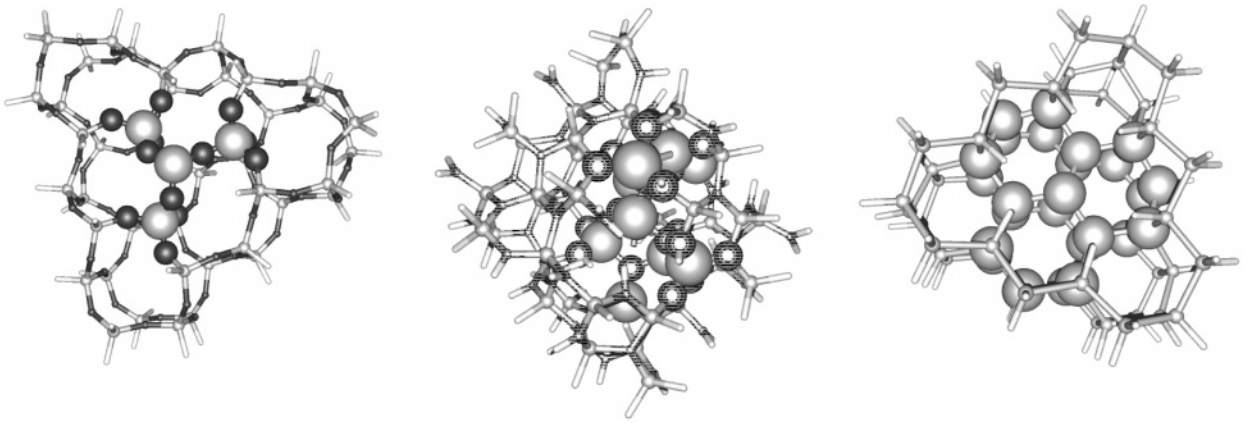

Figure 3. QM/MM models of the $\cdot SiO_3$, $\cdot SiN_3$, and $\cdot SiSi_3$ centers, displayed from left to right. The QM region of each model is the third-nearest neighbor or greater and is illustrated by the portion rendered using a space fill model. The surrounding MM regions are displayed as ball-and-stick models. The silicon radical is located in the center of each picture. Light atoms are silicon, striped atoms are nitrogen, and dark atoms are oxygen. The environment is crystalline in nature.

TABLE 4: Basis Set Dependence of the Hyperfine Coupling Constant (A_0)[a]

basis	isotope	1NN A_0	2NN A_0	3NN A_0
		$-SiO_3$ Cluster		
TZV+d	^{29}Si↑	−537	−459	−452
alt-TZV+d	^{29}Si↑	−527	−451	−445
cc-pVTZ	^{29}Si↑	−481	−418	−411
alt-cc-pVTZ	^{29}Si↑	−517	−450	−442
TZV+d	^{17}O	−58, −55, −46	−42, −42, −34	−41, −37, −33
alt-TZV+d	^{17}O	−57, −41, −40	−41, −41, −34	−40, −37, −33
cc-pVTZ	^{17}O	−53, −50, −42	−38, −38, −31	−37, −34, −30
alt-cc-pVTZ	^{17}O	−53, −49, −42	−38, −38, −31	−37, −34, −30
		$-SiN_3$ Cluster		
TZV+d	^{29}Si↑	−261	−289	−313
alt-TZV+d	^{29}Si↑	−257	−285	−308
cc-pVTZ	^{29}Si↑	−248	−273	−291
alt-cc-pVTZ	^{29}Si↑	−260	−290	−311
TZV+d	^{14}N	8, 14, 14	7, 10, 11	6, 9, 11
alt-TZV+d	^{14}N	8, 14, 14	7, 10, 11	6, 9, 11
cc-pVTZ	^{14}N	7, 13, 13	6, 9, 10	6, 8, 10
alt-cc-pVTZ	^{14}N	8, 14, 14	7, 10, 11	6, 9, 11
		$-SiSi_3$ Cluster		
TZV+d	^{29}Si↑	−75	−78	−72
alt-TZV+d	^{29}Si↑	−76	−78	−73
cc-pVTZ	^{29}Si↑	−78	−81	−75
alt-cc-pVTZ	^{29}Si↑	−77	−79	−75
TZV+d	^{29}Si	4, 4, 5	−1, 2, 8	1, 5, 7
alt-TZV+d	^{29}Si	4, 4, 5	−1, 2, 7	1, 4, 7
cc-pVTZ	^{29}Si	3, 4, 4	−1, 2, 6	1, 4, 6
alt-cc-pVTZ	^{29}Si	3, 4, 4	−1, 2, 6	1, 4, 6

[a] These clusters were built and optimized using the QM/MM scheme and include first-, second-, and third-nearest-neighbor substitution. Hyperfines are reported in units of gauss and were calculated via DFT/B3LYP and the TZV+d basis. The upward arrow symbol (↑) denotes the silicon radical center.

examined are DFT/B3LYP, UHF, and MP2. GAMESS was once again used for these calculations.

Table 4 shows the results of the basis set dependence study using the B3LYP method. The change in the isotropic hyperfines between basis sets for the ^{17}O nucleus in the $\cdot SiO_3$ defect, ^{14}N nucleus in $\cdot SiN_3$, and the ^{29}Si nucleus in $\cdot SiSi_3$ is small ($\leq$5 G). This is due to the low magnitude of the hyperfine interactions for these nuclei. The ^{29}Si nucleus in the $\cdot SiO_3$ and $\cdot SiN_3$ defects have hyperfines larger in magnitude. The change between the altered and original TZV+d basis is slight, 4−10 G. This suggests the TZV+d basis has sufficient flexibility near the nucleus. The hyperfines calculated with the cc-pVTZ basis are significantly less than the previous two basis sets. This change is ∼13−56 G from the TZV+d calculated hyperfine. The altered cc-pVTZ basis remedies this occurrence and produces hyperfines that are within 1−2 G of the TZV+d basis. These results suggest that the main criterion for basis set selection should be flexibility near the nucleus. Basis sets that incorporate more valence description generally do not change the property sufficiently, and the TZV+d basis is reliable.

Similar to previously reported data, the DFT/B3LYP level of theory produces hyperfines that are consistent with second-order Møller−Plesset (MP2) theory. The UHF level of theory was confirmed to overestimate the hyperfine interaction, in comparison to these two levels of theory.

4. Discussion

4.1. Correlation with Experiment. Experimental results for the varying defects investigated in this work are relatively few. The hemi-E′-, K-, P_b-, and X ($\cdot SiO_2Si$)-centers are the only defects in which experimental assignments have been made. The greatest amount of information is available for the hemi-E′- and P_b-centers. These defects have been characterized in silicon-implanted silicon dioxide.[9,10] Variants of the hemi-E′-center with the same composition have been studied in α-quartz[6] (E'_1) and silicon glasses[7] (E'_γ). Also, the P_b-center has been observed in amorphous silicon[8] and Si/SiO_2 systems.[11] The remaining defects are less well-known. The K-centers have been characterized in silicon nitride systems.[12,13] The X-center has also been studied in silicon-implanted silicon dioxide.[9,10] The majority of the nitrogen-containing defects have not been extensively investigated. However, one study has produced ESR/ENDOR spectra, which may contain information on these defects.[25]

Utilizing the third-nearest-neighbor results for the gas-phase-like and QM/MM methods, good correlations with experiment are observed. Changes in the radical environment are observed by the spread of the experimental and calculated hyperfines. Agreement with the experiment is observed in both the magnitude and spread of the calculated isotropic hyperfine coupling constants. The $\cdot SiO_3$ defect is calculated to have a ^{29}Si hyperfine from −452 G to −423 G. This range encloses the experimental results, from 420 to 440 G.[6,7,9,10] The $\cdot SiN_3$ defect also agrees well with the experiment that has ^{29}Si hyperfines from −379 G to −254 G. The experimental value lies within this range at 350 G.[12,13] However, the ^{14}N hyperfine of this defect is a factor of ∼2 too large. The calculated ^{14}N hyperfines are in the range of 7−11 G, with the experiment giving 4.6 G[12,13] as the hyperfine. The $\cdot SiSi_3$ defect is in

agreement with the experimental ^{29}Si hyperfines from 71 G to 111 G.[8−11] The calculated hyperfines for this defect are from −112 G to −72 G. The $\cdot SiO_2Si$ defect has a calculated ^{29}Si hyperfine of −222 G, which agrees with the experimental hyperfine of 230 G.[9,10]

The gas-phase-like and QM/MM models produce isotropic hyperfine coupling constants that are consistent with experiment. The different models are meant to simulate differences in the defect environment as a possible contributing factor to the varying reported hyperfines of these defects. This is well-supported by the comparison of the $\cdot SiSi_3$ defect with experiment. The QM/MM models, which are used with an amorphous or crystalline environment, give better control over the modeled environment than the gas-phase-like models. These gas-phase-like models may give results that are consistent with any environment.

The ^{29}Si hyperfines associated with the first-nearest-neighbor nuclei are, in some cases, calculated to be large (≥30 G). Although these hyperfines are always smaller in magnitude than the ^{29}Si hyperfine associated with the radical nucleus, these signals may be misrepresented as P_b-centers. The $\cdot SiN_2Si$, $\cdot$SiONSi, and $\cdot SiO_2Si$ defects have calculated first-nearest-neighbor ^{29}Si hyperfines from −115 G to −58 G. These fall close to the experimental range of the P_b-centers from 71 G to 111 G. However, the $\cdot SiN_2Si$ and $\cdot$SiONSi defects might be distinguished by the additional ^{14}N splitting of this hyperfine. It is interesting to note that these defects constitute all the defects in which only one Si atom is present in the first-nearest-neighbor shell.

4.2. Trends in Calculated Hyperfines. The overall trends in the calculated isotropic hyperfine coupling constants across types of defects are consistent between the various methods utilized. The absolute value of the hyperfine on the silicon radical nucleus decreases from the $\cdot SiO_3$ to $\cdot SiN_3$ defects, as oxygen is replaced with nitrogen. The hyperfine also decreases, as nitrogen is replaced with silicon, between the $\cdot SiN_3$ and $\cdot SiSi_3$ defects. Conversely, the hyperfine increases between the $\cdot SiSi_3$and $\cdot SiO_3$ defects, as silicon is replaced with oxygen. These trends seem to follow the changes in electronegativity of the first-nearest-neighbor atoms. The O, N, and Si atoms have Pauling electronegativities of 3.44, 3.04, and 1.90, respectively. The largest hyperfines are associated with the $\cdot SiO_3$ defect with all O atoms in its first-nearest-neighbor shell. The smallest hyperfines are associated with the $\cdot SiSi_3$ defect with all Si atoms in its first-nearest-neighbor shell. The $\cdot SiN_3$ defect has an associated ^{29}Si hyperfine intermediate between these two defect centers. The average electronegativity change in the first-nearest-neighbor shell between the $\cdot SiO_3$ and $\cdot SiN_3$ defects is −0.40, −1.14 between the $\cdot SiN_3$ and $\cdot SiSi_3$ defects, and +1.54 between the $\cdot SiSi_3$ and $\cdot SiO_3$ defects. These electronegativity changes follow the same trends as the change in hyperfines.

This correlation between the electronegativity of the first-nearest-neighbor atoms and the hyperfine on the silicon radical nucleus suggests two possible explanations. The change in electronegativity of the first-nearest-neighbor atoms can affect the spin density at the silicon radical nucleus via interaction with the electron density or interaction with the silicon radical's hybridization. The interaction with the electron density (or, more precisely, the spin density) is perceived as a direct delocalization or localization of the radical on a particular nucleus. A more-delocalized radical would have a lower spin density at a particular nucleus and, thus, a lower hyperfine. The interaction with the silicon radical's hybridization is perceived, not as a localization/delocalization phenomenon but as an increase or decrease in a radial's interaction with a nucleus. The spin density at a nucleus is primarily attributed to the spin density in the *s* atomic orbitals. These atomic orbitals are the only function on a nucleus with any density at that nucleus. A change in the radical's *s* character due to changes in hybridization would affect the nuclear spin density. This, in turn, would change the associated hyperfine, according to increasing or decreasing *s* character.

TABLE 5: Pucker of the Central Silicon Radical in QM/MM Models

cluster 3NN	bond angles (deg)			pucker (deg)
$\cdot SiO_3$	111.0	110.5	107.9	30.6
$\cdot SiO_2N$	109.8	108.2	108.1	33.9
$\cdot SiON_2$	113.0	110.2	104.3	32.5
$\cdot SiN_3$	113.9	112.9	108.8	24.4
$\cdot SiN_2Si$	117.0	115.0	112.1	15.9
$\cdot SiNSi_2$	117.8	114.4	113.8	14.0
$\cdot SiSi_3$	119.0	117.8	112.1	11.1
$\cdot SiOSi_2$	116.4	110.2	109.8	23.6
$\cdot SiO_2Si$	108.2	105.7	105.4	40.7
$\cdot$SiONSi	112.1	110.7	108.2	29.0
			planar	0.0
reference			Td	31.5
			Dist Td	60.0

[a] Bond angles of the central silicon radical in studied defects. The clusters were built and optimized using the QM/MM scheme and include third nearest neighbor substitution.

It is not immediately evident that radical localization and hybridization would necessarily be related. However, both are logical rationale for trends in the isotropic hyperfine coupling constants. The trends observed for these defects contradicts a pure electronegativity argument. However, changes in the electronegativity have been shown to change the pucker or $s-p$ hybridization of radicals.[26] The geometrical pucker of these defects is studied to gain insight into the changes in radical hybridization across these defects.

Table 5 reports the bond angles around the central silicon radical. The bond angles are given in units of degrees. The sum of these bond angles gives an estimation of the degree of planarity of the silicon radicals. A 360° sum represents a planar radical, whereas, a 328.5° sum represents an ideally tetrahedral radical. A quantity called the pucker is defined as the bond angle sum minus 360°. A 0° pucker reflects a planar radical, whereas, a 31.5° pucker reflects an ideally tetrahedral radical. The idealized pucker parameters assume equivalent bond angles. This is not generally true. The bond angles reported have at least one bond angle that deviates from the other two bond angles. The change in the silicon radical's pucker is reminiscent of a change in hybridization. A planar radical exhibits no hybridization. The radical is located within an unhybridized p-orbital. An ideally tetrahedral radical exhibits sp^3 hybridization. Generally, the *s* orbital character of the radical increases as the pucker increases. Overall trends in the radical pucker, noting that $\cdot SiO_3$ seems displaced, are consistent with the trends in calculated hyperfines. The pucker decreases between the $\cdot SiO_3$ and $\cdot SiN_3$ defects. Between the $\cdot SiN_3$ and $\cdot SiSi_3$ defects, there is also a decrease. These trends suggest a reduction of *s* orbital character proceeding in this direction. This is in agreement with the observed decrease in hyperfine. The pucker increases between the $\cdot SiSi_3$ and $\cdot SiO_3$ defects. This trend is also in agreement with observed hyperfines. The change in hybridization of the silicon radical nucleus due to changing pucker is the primary factor that affects the calculated hyperfines.

The similar trends observed for the first-nearest-neighbor nuclei give further evidence of the correlation between hybridization and hyperfines. These similar trends suggest a through-bond interaction of these nuclei with the radical. This situation would definitely be affected by changes in hybridization.

5. Conclusion

Calculation of the isotropic hyperfine coupling constant was performed on gas-phase-like and quantum mechanical/molecular mechanical (QM/MM) models of the possible paramagnetic silicon defects in silicon oxynitride. The ^{29}Si hyperfine associated with the central silicon radical was observed to be dependent on the identity of its first-nearest neighbors. This dependence follows trends in the electronegativity of these atoms and was verified to result from a change in radical hybridization across these defects. The trends in hyperfines also extend to the first-nearest-neighbor atoms, which suggests a through-bond interaction.

Agreement with the experiment is observed between the various models utilized in this study. The effect of environment incorporated via QM/MM extended models is a geometric effect that explains the differing experimental values for some defects. The QM/MM methods give better control of this environmental effect than does the gas-phase models. The calculated isotropic hyperfines of defects not known experimentally are of benefit to future experimental studies on these materials.

References and Notes

(1) Wilk, G. D.; Wallace, R. M.; Anthony, J. M. *J. Appl. Phys.* **2001**, *89*, 5243.

(2) Nishi, Y. *Jpn. J. Appl. Phys.* **1966**, *5*, 333.

(3) Nishi, Y. *Jpn. J. Appl. Phys.* **1971**, *10*, 52.

(4) Fleetwood, D. M.; Warren, W. L.; Schwank, J. R.; Winokur, P. S.; Shaneyfelt, M. R.; Riewe, L. C. *IEEE Trans. Nucl. Sci.* **1995**, *42*, 1698.

(5) Zvanut, M. E.; Feigl, F. J.; Fowler, W. B.; Rudra, J. K.; Caplan, P. J.; Poindexter, E. H.; Zook, J. D. *Appl. Phys. Lett.* **1989**, *54*, 2118.

(6) Weeks, R. A. *J. Appl. Phys.* **1956**, *27*, 1376.

(7) Griscom, D. L.; Friebele, E. J.; Sigel, G. H., Jr. *Solid State Commun.* **1974**, *15*, 479.

(8) Yokomichi, H.; Hirabayashi, I.; Morigaki, K. *Solid State Commun.* **1987**, *61*, 697.

(9) Hosono, H.; Kawazow, H.; Oyoshi, K.; Tanaka, S. *J. Non-Cryst. Solids* **1994**, *179*, 39.

(10) Mizuguchi, M.; Hosono, H.; Kawazoe, H. *Mater. Sci. Eng., B* **1998**, *54*, 38.

(11) Brower, K. L. *Appl. Phys. Lett.* **1983**, *43*, 1111.

(12) Lenahan, P. M.; Curry, S. E. *Appl. Phys. Lett.* **1990**, *56*, 157.

(13) Warren, W. L.; Lenahan, P. M. *Phys. Rev. B* **1990**, *42*, 1773.

(14) Karna, S. P.; Kurtz, H. A.; Shedd, W. M.; Pugh, R. D.; Singaraju, B. K. *IEEE Trans. Nucl. Sci.* **1999**, *46*, 1544.

(15) Pacchioni, G.; Erbetta, D. *Phys. Rev. B* **1999**, *60*, 12617.

(16) Hermosilla, L.; Calle, P.; García del la Vega, J. M.; Sieiro, C. *J. Phys. Chem. A* **2005**, *109*, 1114.

(17) Hermosilla, L.; Calle, P.; García del la Vega, J. M.; Sieiro, C. *J. Phys. Chem. A* **2005**, *109*, 7626.

(18) (a) Becke, A. D. *J. Chem. Phys.* **1993**, *98*, 5648. (b) Stephens, P. J.; Devlin, F. J.; Chablowski, C. F.; Frisch, M. J. *J. Phys. Chem.* **1994**, *98*, 11623. (c) Hertwig, R. H.; Koch, W. *Chem. Phys. Lett.* **1997**, *268*, 345.

(19) (a) Binkley, J. S.; Pople, J. A.; Hehre, W. J. *J. Chem. Phys.* **1980**, *102*, 939. (b) Stevens, W. J.; Basch, H.; Krauss, M. *J. Chem. Phys.* **1984**, *81*, 6026.

(20) (a) Pietro, W. J.; Francl, M. M.; Hehre, W. J.; DeFrees, D. J.; Pople, J. A.; Binkley, J. S. *J. Am. Chem. Soc.* **1982**, *104*, 5039. (b) Dobbs, K. D.; Hehre, W. J. *J. Comput. Chem.* **1986**, *7*, 359. (c) Hariharan, P. C.; Pople, J. A. *Theor. Chim. Acta* **1973**, *28*, 213. (d) Gordon, M. S. *Chem. Phys. Lett.* **1980**, *76*, 163. (e) Francl, M. M.; Pietro, W. J.; Hehre, W. J.; Binkley, J. S.; Gordon, M. S.; DeFrees, D. J.; Pople, J. A. *J. Chem. Phys.* **1982**, *77*, 3654.

(21) (a) Maseras, F.; Morokuma, K. *J. Comput. Chem.* **1995**, *16*, 1170. (b) Shoemaker, J. R.; Burggraf, L. W.; Gordon, M. S. *J. Phys. Chem. A* **1999**, *103*, 3245. (c) Ponder, J. W.; Richards, F. M. *J. Comput. Chem.* **1987**, *8*, 1016. (d) Kundrot, C. E.; Ponder, J. W.; Richards, F. M. *J. Comput. Chem.* **1991**, *12*, 402.

(22) Schmidt, M. W.; Baldridge, K. K.; Boatz, J. A.; Elbert, S. T.; Gordon, M. S.; Jensen, J. J.; Koseki, S.; Matsunaga, N.; Nguyen, K. A.; Su, S.; Windus, T. L.; Dupuis, M.; Montgomery, J. A. *J. Comput. Chem.* **1993**, *14*, 1347.

(23) (a) Dunning, T. H. *J. Chem. Phys.* **1971,** *55*, 716. (b) McLean, A. D.; Chandler, G. S. *J. Chem. Phys.* **1980**, *72*, 5639.

(24) (a) Dunning, T. H. Jr. *J. Chem. Phys.* **1989**, *90*, 1007. (b) Woon, D. E.; Dunning, T. H. Jr. *J. Chem. Phys.* **1993**, *98*, 1358. (c) Basis sets were obtained from the Extensible Computational Chemistry Environment Basis Set Database, Version 02/25/04, as developed and distributed by the Molecular Science Computing Facility, Environmental and Molecular Sciences Laboratory, which is part of the Pacific Northwest Laboratory, P.O. Box 999, Richland, WA 99352, and funded by the U.S. Department of Energy. The Pacific Northwest Laboratory is a multiprogram laboratory operated by Battelle Memorial Institute for the U.S. Department of Energy, under Contract No. DE-AC06−76RLO 1830. Contact Karen Schuchardt for further information.

(25) Yokomichi, H.; Kondo, M.; Morigaki, K. *J. Non-Cryst. Solids* **1989**, *114*, 426.

(26) Cooper, J.; Hudson, A.; Jackson, R. A. *Mol. Phys.* **1972**, *23*, 209.